Electronic Supplementary information (ESI) *for*

Oxidation dependent Atomic Structures and Electrooxidation Activities of Carbon Supported Platinum-Ruthenium Catalysts

Authors: Po-Chun Huang,[a] Hong-Shuo Chen,[b] Yu-Ting Liu,[c] I-Li Chen,[b] Sheng-Yang Huang,[e] Ha M. Nguyen,[a] Chi-Chang Hu,[d] Kuan-Wen Wang,[b] and Tsan-Yao Chen[a,]*

Affiliations:

a Department of Engineering and System Science, National Tsing Hua University, Hsinchu 30013, Taiwan

b Institute of Materials Science and Engineering, National Central University;

c Department of Environmental Science and Engineering, Tunghai University, Taichung 40704, Taiwan

d Department of Chemical Engineering, National Tsing Hua University, Hsinchu 30013, Taiwan

e Department of Chemical Engineering, University of South Carolina, Columbia, SC 29208, USA

*To whom the correspondence should be addressed. E-mail: chencaeser@gmail.com

Fax: 886-3-5720724

S1. X-ray Diffraction Characterization.

For XRD, the samples were deposited on a Si (100) wafer and dried at the lab atmosphere for 6h. The XRD patterns were collected on a Mac‐Science MXP18 diffractometer equipped with a diffraction beam monochromator and a rotation anode Cu target X‐ray tube (40 kV and 100 mA). The spectra were collected from 20° to 80° in 0.02° increments and 3 s/point. The coherent length of the $Pt-Ru/C$ nanocatalysts was estimated from the XRD pattern using the Scherrer equation (eq. S1)[1, 2].

$$t = \frac{K\lambda}{B\cos\theta} \qquad \text{(S1)}$$

where t is the particle size, K is the shape factor (0.9), λ is the X‐ray wavelength (1.54 Å), B is the full width of the halfmaximum (FWHM) for the XRD peak, and θ is the Bragg angle. The TEM used was a field-emission gun JEOL JEM 2100, operated at 200 kV, and the images were captured with a Hamamatsu ORCA-HR digital camera. The samples were dispersed in ethanol and deposited onto a Formvar/carbon ‐coated 300 mesh Cu grid and dried in a N_2 filled grove box for at least 30 min prior to observation. TPD and TGA studies of the $Pt-Ru/C-H_2$ and blank carbon samples were performed to monitor thermal desorption of metal precursors and carbon oxidation of Pt-Ru/C-H_2. An alumina pan was used with a ramp rate of 10 K min^{-1} from 300 to 1200 K in air flow (50 mL min^{-1}). A Agilent 5975 Series MSD real time

gravimetric analyzer was used.

Table S1. XRD determined Structure parameters of Pt-Ru/C-To

S2. X-ray absorption spectroscopy measurements.

Pt L_3 – edge (11564 eV) and Ru K – edge (22117 eV) data were collected at the Wiggler (W20 BL – 17C) beamline and Superconducting Wavelength Shifter (SWLS BL – 01C1) beamline of the Taiwan Light Source (TLS, operated at 1.5 GeV) in the National Synchrotron Radiation Research Center (NSRRC), Taiwan. Both the two beamlines are equipped with Fixed-Exit Double Crystal Si(111) Monochromator and a Toroidal Focusing Mirror. The W20 beamline has an energy range of 5 – 12 keV and the SWLS beamline energy range is 6 – 33 keV. The samples were loaded into an alumina oxide cell and the spectra were collected using transmission mode.

S2.1 X-ray absorption data analysis

The XAS data normalization and analysis were conducted using the Athena package in the IFEFFIT program.[3, 4] The atomic coordinates used in the FEFF6.0 input files were taken from models of metallic platinum (Pt) (ICSD #041525), rutile platinum oxide (PtO) (ICSD #26599), cubic platinum chlorite ($PtCl_3$) (ICSD #22073),

and rutile ruthenium oxide (RuO_2) (ICSD #15071) (Scheme S1), which were created in the Artemis program. Metallic platinum (Scheme S1a) has first nearest neighbors located at 2.77 Å, corresponding to a coordination number (CN) of 12. Rutile RuO_2 (Scheme 1b) has a central Ru atom that is octahedral coordinated to sox surrounding O atoms; four at 1.98 Å and two at 1.94 Å. The shortest $Ru-Ru$ distance is 3.11 Å along the c axis of the unit cell, with a CN of 2. The next shortest $Ru-Ru$ is 3.53 Å from the central Ru to the corner Ru atoms and thus corresponding to a CN of 8.[5] For Ru L-edge calculations, the FEFF6 program produced a list of theoretical phase shifts and amplitudes that were used in the EXAFS fitting of the experimental data. Artemis (FEFFIT) was used to extract the EXAFS signal, $\chi(k)$, based on the following equation (eq. S2):

$$\chi(k) = \frac{\mu(k) - \mu_0(k)}{\mu_0(k)} \qquad \text{(S2)}$$

where k is the photoelectron wavevector $[k = (2m/\hbar^2(E - E_0))^{1/2}]$, $\mu(k)$ is the measured X-ray absorption coefficient, and $\mu_0(k)$ is a spline fit of the EXAFS region. Structural parameters were obtained from the experimental EXAFS data by a nonlinear least-squares fit of the theoretical $\chi(k)$, which was conducted in R space by Fourier transforming $\chi(k)$.

S2.2. Compositional analysis of XANES by linear combination method

The compositions of NCs are determined by fitting their corresponding Pt L_3－edge and Ru K－edge XANES using a linear combination method. The fitting photon energy was selected from －20 to 20 eV relative to the absorption edge. The results are extracted by fitting experiment data with the weighting factors "$a_{i(ox)}$" of a series of standard i compound spectra ($\mu(E)_{i(ox)}$) in different oxidation states (see eq. S3):

$$\mu(E)_{(To,i)} = \sum a_{i(ox)} \cdot \mu(E + \Delta E)_{i(ox)} \qquad \text{(S3)}$$

where $\mu(E)_{(To,i)}$ denotes the XANES spectra of the $Pt-Ru/C-T_o$ sample and ΔE is the spectra edge shift between the standard i compound and the $Pt-Ru/C-T_o$ samples.

Data collection of X－ray absorption spectra (XAS). The Pt L_3－edge (11564 eV) and Ru K－edge (22117 eV) XAS spectra of $Pt-Ru/C$ catalysts were recorded using the wiggler beamline at BL－17C1 and the superconducting wavelength shifter beamline at BL－01C1 of National Synchrotron Radiation Research Center (Hsinchu, Taiwan), respectively. The 1.5 GeV electron storage ring was operated on Top－Up mode with an injection period in 60 second The beam current (I_0) is 360 mA with a small current variation ($\Delta I_0/I_0$) of 0.05 %. Three gas－filled ion chambers were used in series to measure the intensities of the incident beam (I_0), the beam transmitted across the sample (I_t), and the beam subsequently transmitted across the reference foil

(I_r). The third ion chamber was used in conjunction with the reference spectra of standard samples ($\mu_t^{ref} = ln(I_t/I_r)$) of Pt foil and Ru powder for energy calibration at Pt L_3-edge and Ru K-edge, respectively. All the Pt L_3 and Ru K-edges XAS spectra of prepared samples were collected in a transmission mode, i.e. $\mu_t^{exp} = ln(I_0/I_t)$. Due to the low penetration depth of tender X-ray (normally less than 100 μm ranging from 2 to 4.5 keV), the XAS data at Ru L_3-edge were collected using the fluorescence mode ($\mu_t^{exp} = I_f/I_0$) by a Lytle detector with an incident X-ray monochromator detuned 30% to avoid the high order harmonic photons from (111) reflection of Si monochromator.

Data Subtraction of Pt L_3 and Ru K-edge XAS. The XAS data including the XANES and the EXAFS oscillations ($\chi(k)$), where k is the photoelectron wave number, were extracted and normalized according to the standard procedures of Athena program (with the code of AUTOBK algorithm 2.93) in the IFEFFIT package (version 1.2.10).[6-9] Using a Hanning window function forward Fourier transformation (FFT) was performed on the EXAFS region of normalized XAS spectra with the selected k ranges for the Pt L_3 (from 3.25 Å^{-1} to 14.1 Å^{-1}) and Ru K-edges (from 2.85 Å^{-1} to 13.90 Å^{-1}) to generate the radial structure functions (RSF) in the radial space ranging from 1.0 Å to 5.0 Å.

XAS data analysis (model fitting). To conduct a XAS simulation, the reference structural information of standard Pt, PtO_2, Ru, and RuO_2 crystals (obtained from the Inorganic Crystal Structure Database (ICSD) and WebAtoms Database) was implemented in FEFF6.20 program[10] in the IFEFFIT package (version 1.2.10)[6-8] to generate theoretical bond paths of $Pt-Pt$, $Pt-Ru$, $Pt-O$, $Ru-O$, $Ru-Ru$, and $Ru-Pt$. The model of simulating Pt L_3 – edge XAS data was based on the cadre of Pt FCC crystal (with a crystal $Fm\bar{3}m$ symmetry), where the number of neighboring atoms in the nearest shell (N_{Pt-N}) is 12 at the interatomic distance (R_{Pt-N}) of 2.772 Å. The bond path of heteroatoms was generated by substituting Pt with Ru in the first coordination shell of the lattice model. Furthermore, the $Pt-O$ paths were created from the FEFF6.01 code[11] using the structural information of PtO_2 in the Inorganic Crystal Standard Database (ICSD).[12] Model of RuO_2 structure was referred to the standard information depicted by Boman, C. E. (1970).[13]

The obtained RSF function was analyzed using EXAFS simulation (Artemis kits) with appropriate models (the scattering paths of $Pt-Pt$, $Pt-Ru$, and $Ru-Ru$ bonding pairs) to investigate the local structural parameters (including the structural parameters of interatomic bond distance (R_{ij}), phase shifts (Φ_{ij}), coordination numbers (N_j), amplitude reduction factor (S_i^2), effective wave backscattering amplitude ($F_j(k)$),

and Debye – Waller factor (σ_j^2)) around X – ray excited atoms in IFEFFIT program with EFEE6.01 code.[3, 4, 14] To simplify the EXAFS fitting, the values of S_i^2 of Pt and Ru atoms were fixed at 0.83 which was in good agreement with the theoretical estimation and can be used for different samples with central atoms in a similar chemical state (valence, coordination). Only single scattering paths were considered in fitting the experimental XAS data to prevent unexpected analytical errors (which may be due to the background noises or the multiple scattering effects from the higher order shells). The model simulation of XAS fitting with metal substitution was conducted by incorporating appropriate constrains in a single coordination shell. To evaluate the local structural information around X – ray excited atoms, we adopted independent iterations to avoid the unexpected errors of direct correlation between structural parameters. The $k^3\chi(k)$ were fitted with all the possible scattering paths for the corresponding FT peaks, where structural parameters of σ_j^2, N_j, and the R_{ij} were treated as adjustable parameters.[15]

For Ru K – edge EXAFS analysis, the k-space data (k designates the wave vector of photoelectrons) were Fourier transformed (FT) over the range of 2.8 Å^{-1} – 12.7 Å^{-1}, and the offset FT[$\chi(k)*k^3$] for each oxidation temperature is shown in Figure S1(a). As with the XANES spectra, the $Pt-Ru/C-H_2$ FT spectrum is very similar to that seen in literature for metallic Ru and $RuCl_3$. The spectra for the 300 K and 370 K are more

similar to that of heavily hydrated RuO_2[16, 17] whereas the spectra for the 470 K and 520 K are similar to those of slightly hydrated RuO_2 samples. Finally, the 570 K spectrum resembles that of anhydrous RuO_2 samples. For low temperature oxidized samples (as prepared, 300 K, and 370 K), a short *k* range for the FT results in poorer resolution of the $Ru-Ru$ peaks (ranged from 3.11 Å to 3.54 Å) in the R space than a longer k range would. This is because the low counting statistics in the high *k* range and can explain discrepancies between the R-space spectra seen here and seen in literature. It should be noted that most of the spectra collected allow for a longer *k* range to be used for the FT. However the lowest quality spectra, 300 K, is noisy above k = 12.7 $Å^{-1}$ and thus all spectra are presented with this range for consistency. The R-space spectrum for the $Pt-Ru/C-H_2$ sample appears to have contributions from both metallic Ru ($Ru-Ru$ peak at 2.26 Å)[17, 18] and $RuCl_3$ (at 1.96 Å as a shoulder in the left of $Ru-Ru$ peak) as those seen in literature and the 300 K spectrum is similar to that of orthorhombic RuO_2. For high temperature samples (370 K, 470 K, 520 K, and 570 K), the R-space spectra appears to have contributions from monoclinic and rutile RuO_2. Therefore, Figure S1(a) confirms that, comparing with results of TGA/TPD – MS and XRD, the Ru species of NPs in the $Pt-Ru/C$ samples transition from metallic Ru ($Pt-Ru/C-H_2$) clusters to hydrated orthorhombic RuO_2 clusters (amorphous) at ca. 300 K and from amorphous RuO_2 to anhydrous rutile/monoclinic

RuO_2 NPs at ca. 370 K to 570 K. In Figure S1(a), as the oxidation increases from 300 K to 470 K, there is a slight incrase in intensity of the $Ru-O$ peak at 1.2 Å, indicating that the octahedral $Ru-O$ shell becomes more ordered. In addition, there is a slight increase in intensity at ca. 2.7 Å – 2.8 Å, which will be discussed in the R-space fitting results below. The 300 K to 470 K spectra also have a decrease intensity at 2.2 Å, relative to the other spectra in this plot, which has been attributed to $Ru-OH$ bonds in highly hydrated RuO_2. Also seen in Figure S1(a) is that as the oxidation temperature is increased from 470 K to 570 K. The intensities of the peaks increase substantially, indicating that the structure of tettragonal RuO_2 becomes more ordered as expected.

The evolutions of Pt atomic structure in $Pt-Ru/C$ were elucidated by Pt L_3 – edge EXAFS analysis. Figure S1(b) shows the Pt L_3 – edge offset FT[$\chi(k)*k^3$] for each oxidation temperature sample without phase correction. As presented, the $Pt-Ru/C-H_2$ FT spectrum is similar to that of contributions from tetragonal Pt oxide ($Pt-O$ at 1.71 Å), cubic $PtCl_4$ ($Pt-Cl$ at 2.11 Å), and metallic Pt ($Pt-Pt$ at 2.78 Å). The spectra for the 300 to 370 K are similar to that of contributions from tetragonal PtO and cubic $PtCl_4$.[12, 19] The spectra of high temperature samples (470 K to 520 K) appear to have the contributions from mainly hexagonal PtO_2,[20] cubic $PtCl_4$, and possibly slightly metallic Pt. The peak resulting from $Pt-O$ is less intense in the

spectrum of 550 K than that of 520 K (see the overlain of spectra in Figure S3(a)). This, consistent with the result of compositional analysis, suggesting that the decomposition of PtO_2 due to the fact the Pt atoms tends to restructure themselves into clusters to decrease the surface free energy.[21] An even clear feature for the PtO_2 decomposition and Pt restructure is shown by the substantial enhanced $Pt-Pt$ peak in 570 K spectrum. These observation indicates that the freshly prepared sample contains a thin layer of metallic Pt atoms and retained Pt chlorite at surface. For oxidized catalysts, the 300 K and 370 K samples are predominated mainly by PtO, with a small amount of $PtCl_4$ present (2.15 Å to 2.21 Å). The 470 K and 520 K spectra has a substantial intense $Pt-O$ peak than 300 K and 370 K spectra and they have a decreased intensity at 2.15 Å, where the $PtCl_4$ peak should be located. This suggests that there is a transition PtO to PtO_2 transition from 370 K to 470 K. Upon the transition, the retain chlorite would be oxidized and then be decomposed from the bimetallic NPs. A further oxidation at 570 K substantially restructures and decomposes the PtO_2 into metallic Pt clusters.[22-24] Figure S3(b) shows the overlain 570 K and polymer blended 4.2 nm Pt NPs. The peak resulting from metallic Pt (across 2.6 Å to 2.7 Å) are less intense in the 570 K than the Pt NPs spectrum. Since the average size for metallic domains in 570 K was determined to be ~8.5 nm from XRD and TEM, these observations suggest that the 570 K sample contains NPs that

are rich with local disorders, with a small amount of metallic Ru present, and have substantial extent of direct contact with heterogeneous interface of RuO_2 regions.[25]

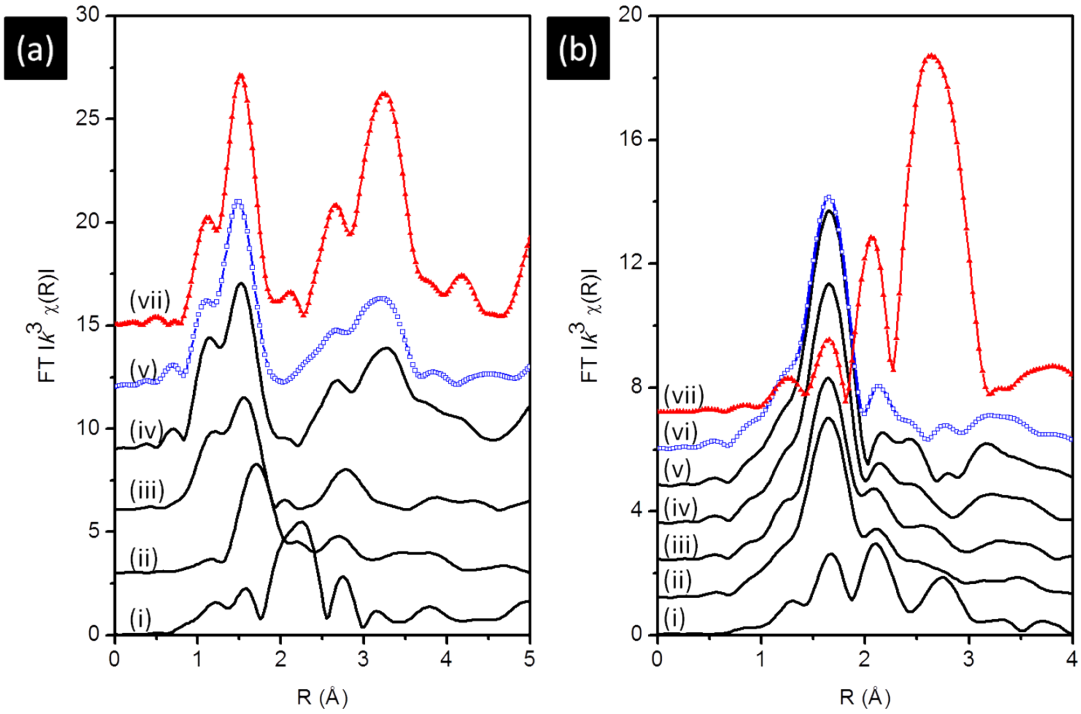

Figure S1. R – space spectra of all catalysts at (S1a) Ru K – edge and (S1b) Pt L_3 – edge R – space spectra.

S2.3 Compositional analysis by XANES fitting.

The $Pt-Ru/C$ contains both non-reacted precursors ($PtCl_4$ and $RuCl_3$) and products ($Pt-Ru$ bimetallic NPs, PtO_2, and RuO_2, etc.), and the relative amounts of each species can be determined by compositional analysis of the XANES region using Athena package in ifeffit program. For Ru K – edge analysis, the metallic Ru powder, RuO_2 and $RuCl_3$ were used as the reference in the fitting because these species are presumably coexisting in the bimetallic NPs (in different ratios associating with

oxidation temperatures). The 570 K sample was used as the hydrous RuO_2 reference for the same reasons. The compositional fits were performed over the range of 22.08 to 22.15 keV.

Table S1 shows the compositional fitting results of all presenting $Pt-Ru/C-T_o$ samples (the XANES spectra comparing with their fitting curves are shown in Figure S2). From Ru K^- edge data, the obtained results indicate that the $Pt-Ru/C-H_2$ sample presents ca. 62.7% metallic Ru and 35.7% $RuCl_3$. The 300 K samples has Ru present as ca. 18.6% Ru metal, 13.7% $RuCl_3$, and 67.7% RuO_2, respectively. This composition difference consistently meets the rapid oxidation trend of ruthenium species (including metallic Ru, $RuCl_3$, and possibly other compounds). For high temperature samples (470 K to 570 K), the total amounts of metallic Ru and $RuCl_3$ were further decreased to less than 10%. This raises the issues as to whether there is one type of particle present, containing on average these ratios between the three species or whether there are three types of particles present (i.e., the mixture of metallic Ru NPs, $RuCl_3$ cluster, and RuO_2 NPs). These two issues are clarified in the Ru K^- edge EXAFS. Meanwhile, the compositional values correlated well with the observed contributions in the R space spectra for these samples below.

From Pt L_3^- edge data, the $Pt-Ru/C-H_2$ contains ca. 69.8% metallic Pt, 11.6% $PtCl_4$, and 18.6% PtO_2, respectively. The 300 K and 370 K samples have Pt present as

ca. ~39 – 41% Pt metal, 15 – 18% $PtCl_4$, and 42 – 43% PtO_2, respectively. Comparing to 370 K sample, a drastic metallic Pt decrease (20 – 40%) was found in 470 K and 520 K samples. Given that these two samples have similar $PtCl_4$ contents (15 – 23%), we can suggesting that the $PtCl_4$ oxidation might by hindered by the competition of $RuCl_3$ and Ru oxidation. Finally, the 570 K sample has 80% metallic Pt, 9.4% $PtCl_4$, and 6.7% PtO_2, respectively. This directly refers to the transition of Pt oxides to metallic Pt, which is consistently probed by above XRD results and the XAS analysis in below.

The chemical species distribution also reveals the oxygen pathways in $Pt-Ru/C-T_o$. This information explains how local mass changes in NCs and, when combining with the results of TGA and TPD – MS, confirms that the oxygen atoms diffuse from NCs surface to interact with carbon support. Here, the weight distribution of chemical species in Pt-Ru/C under different oxidation temperature is shown in Figure S4 using results of Table S1. The weight loss of carbon supported NCs were estimated using chemical stoichiometries (see chemical reactions in eq. S4 – S7) with results of chemical distributions as determined via linear combination analysis:

$$Pt + PtCl_4 + O_2 = PtO_2 + PtCl_4^R + Pt^R + Cl_2 \ldots (S4)$$

$$Ru + RuCl_3 + O_2 = RuO_2 + RuCl_3^R + Ru^R + Cl_2 \ldots (S5)$$

where $PtCl_4^R$, $RuCl_3^R$, $Pt^R$and Pt^R refers to the remaining reactants in eq. S4 and eq. S5, respectively. The total weight of Pt (Ru) species in $Pt-Ru/C-T_o$ denoted as $T_oW_{Pt\_total}$ ($T_oW_{Ru\_total}$) was determined using following equations:

$$T_oW_{Pt\_total} = C_{(PtO2)} \times [PtO_2] + C_{(PtCl4)} \times [PtCl_4] + C_{(Pt)} \times [Pt] \quad (S6)$$

$$T_oW_{Ru\_total} = C_{(RuO2)} \times [RuO_2] + C_{(RuCl3)} \times [RuCl_3] + C_{(Ru)} \times [Ru] \quad (S7)$$

where C(i) refers to the mole ratio of chemical species (i) in eq. S6 and S7 with a molecular weight of [i]. Within estimations, the mole ratio of "i" species was adopted from results shown in Table S1. As shown in Figure S4, the total weights of Pt with Ru species increased by 24 – 37 mg, elucidating the weight loss originates from the combustion of carbon support after 1000 mg of catalyst powder being oxidized at $T_o > 300$ K. Accordingly, the substantial carbon combustion again rationalizes the easy dissociation of oxygen molecule with a subsequent diffusion of oxygen atoms at NCs surface followed by the reaction between oxygen atoms and carbon support at the heterogeneous interfaces.[22]

Table S2. Compositional analysis fits of the Ru K − edge and Pt L_3 − edge XANES regions for the $Pt-Ru/C-T_o$ samples.

Sample	Pt L_3 − edge	Ru K − edge

	Pt^0	$PtCl_4$	PtO_2	Ru^0	$RuCl_3$	RuO_2
Pt-Ru/C-H_2	69.8	11.6	18.6	62.7	35.7	NA
Pt-Ru/C-300	39.3	18.2	42.5	18.6	13.7	67.7
Pt-Ru/C-370	41.6	15.1	43.3	24.7	8.9	88.4
Pt-Ru/C-470	23.9	15.7	60.4	1.6	7.5	90.9
Pt-Ru/C-520	11.2	23.5	65.4	2.7	2.2	95.7
Pt-Ru/C-570	84.0	9.4	6.7	2.0	7.3	90.7

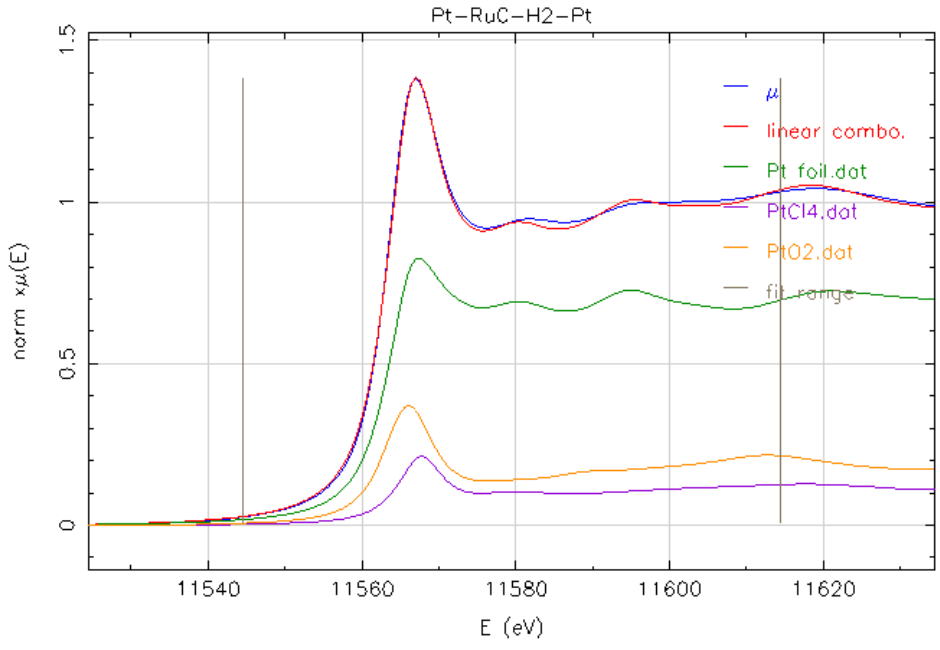
Pt–RuC–H2–Pt
norm xμ(E)
E (eV)
μ
linear combo.
Pt foil.dat
PtCl4.dat
PtO2.dat
fit range

(a)

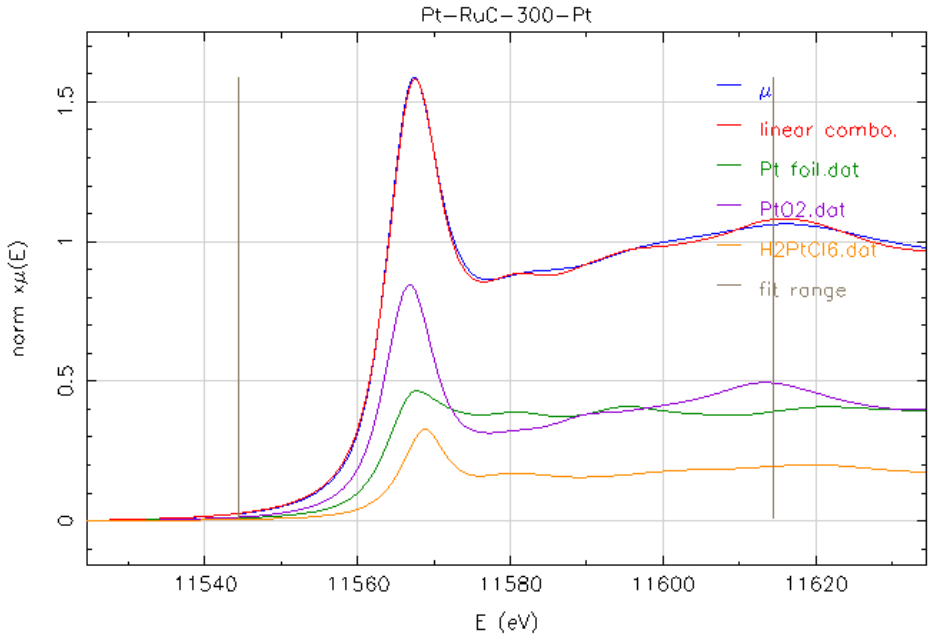
Pt–RuC–300–Pt
norm xμ(E)
E (eV)
μ
linear combo.
Pt foil.dat
PtO2.dat
H2PtCl6.dat
fit range

(b)

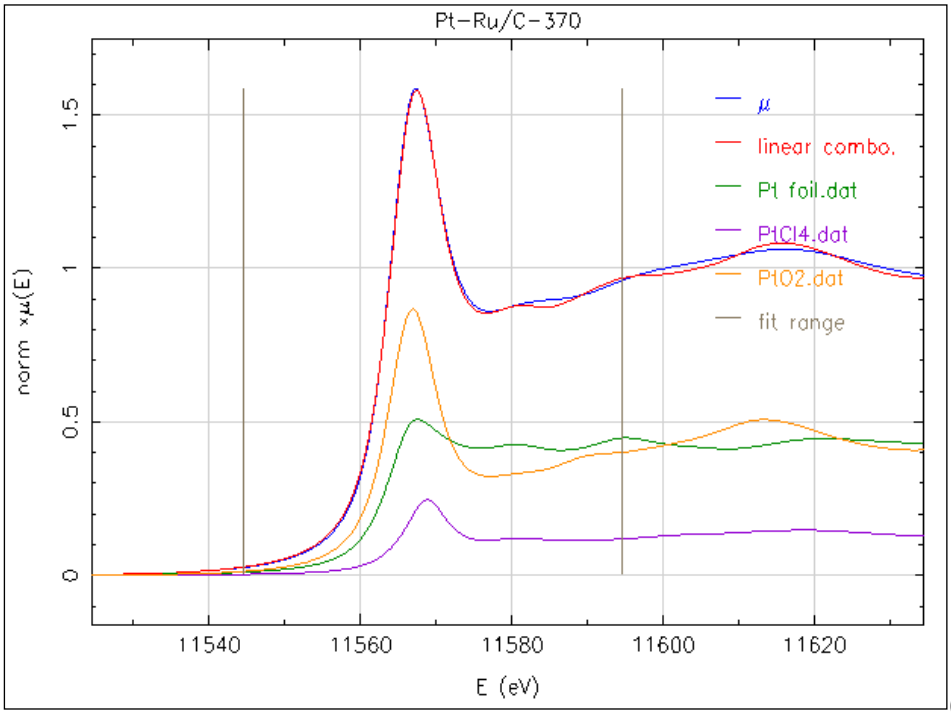
Pt-Ru/C-370
μ
linear combo.
Pt foil.dat
PtCl4.dat
PtO2.dat
fit range
norm xμ(E)
0
0.5
1
1.5
11540
11560
11580
11600
11620
E (eV)

(c)

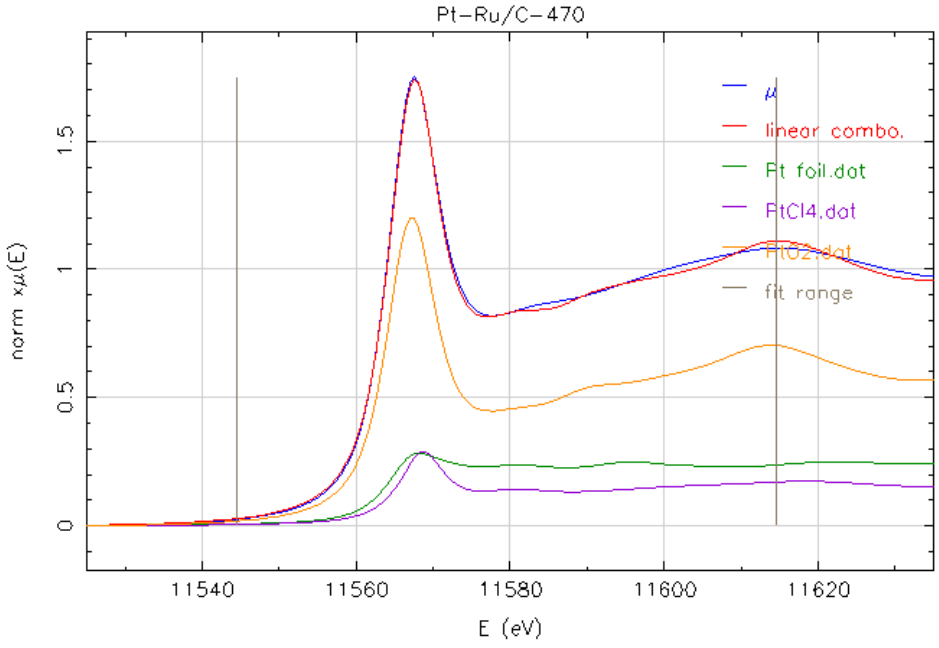
Pt-Ru/C-470
μ
linear combo.
Pt foil.dat
PtCl4.dat
PtO2.dat
fit range
norm xμ(E)
0
0.5
1
1.5
11540
11560
11580
11600
11620
E (eV)

(d)

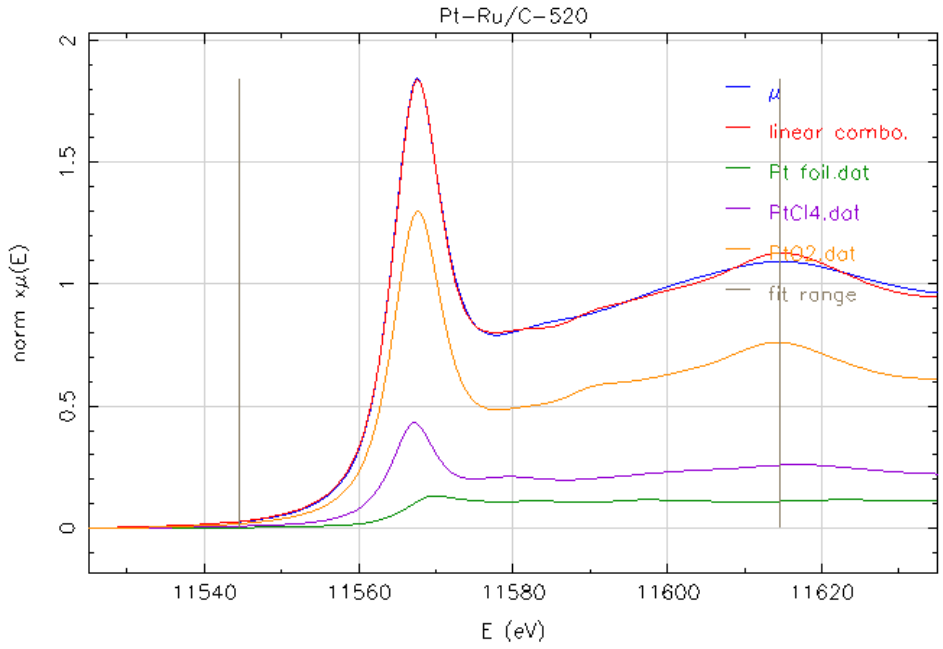
Pt-Ru/C-520
norm xμ(E)
E (eV)
μ
linear combo.
Pt foil.dat
PtCl4.dat
PtO2.dat
fit range

(e)

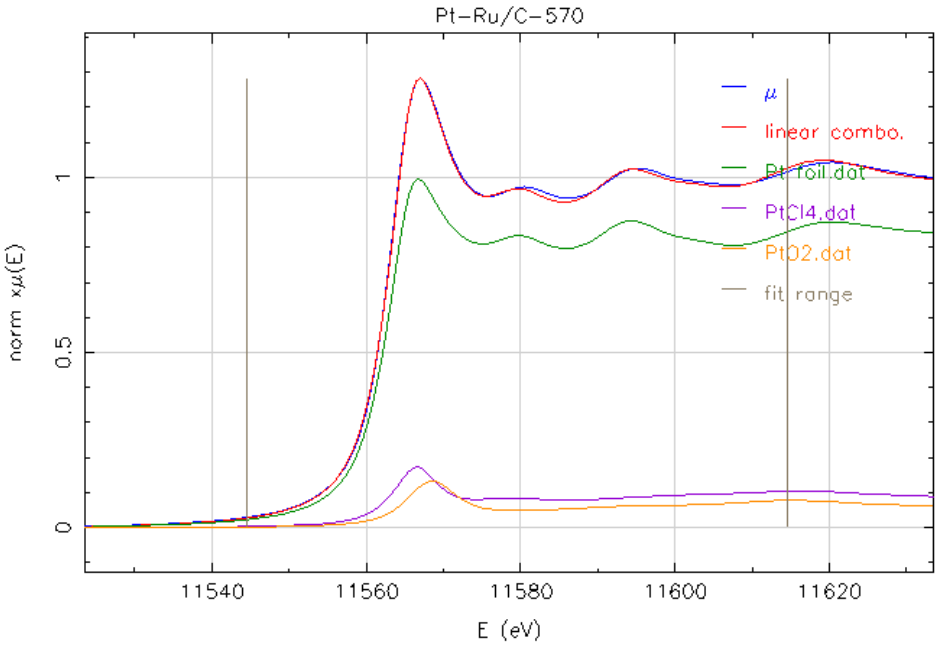
Pt-Ru/C-570
norm xμ(E)
E (eV)
μ
linear combo.
Pt foil.dat
PtCl4.dat
PtO2.dat
fit range

(f)

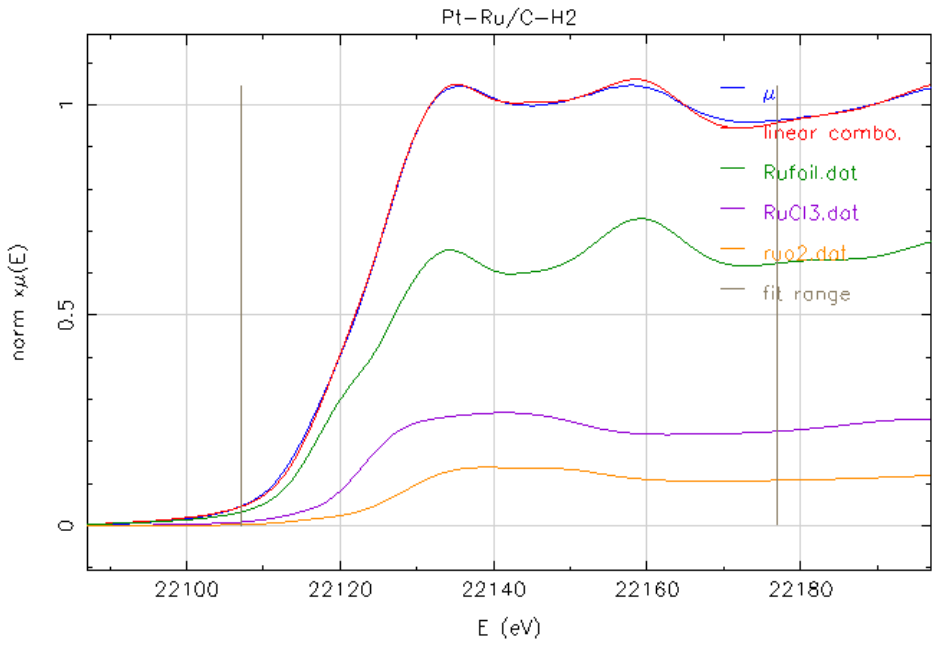
Pt-Ru/C-H2
μ
linear combo.
Rufoil.dat
RuCl3.dat
ruo2.dat
fit range
norm xμ(E)
0
0.5
1
22100
22120
22140
22160
22180
E (eV)

(g)

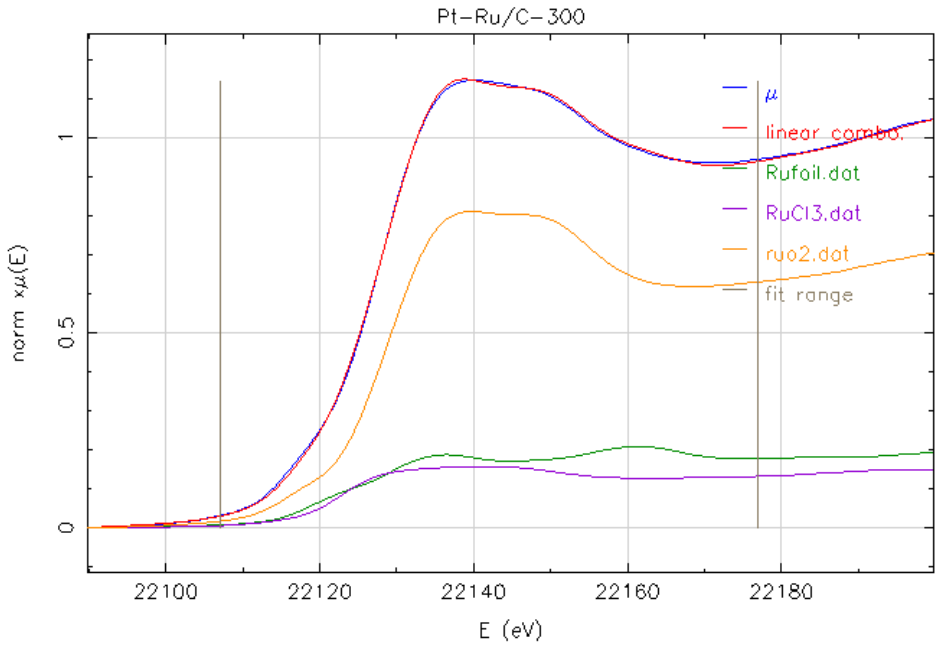
Pt-Ru/C-300
μ
linear combo.
Rufoil.dat
RuCl3.dat
ruo2.dat
fit range
norm xμ(E)
0
0.5
1
22100
22120
22140
22160
22180
E (eV)

(h)

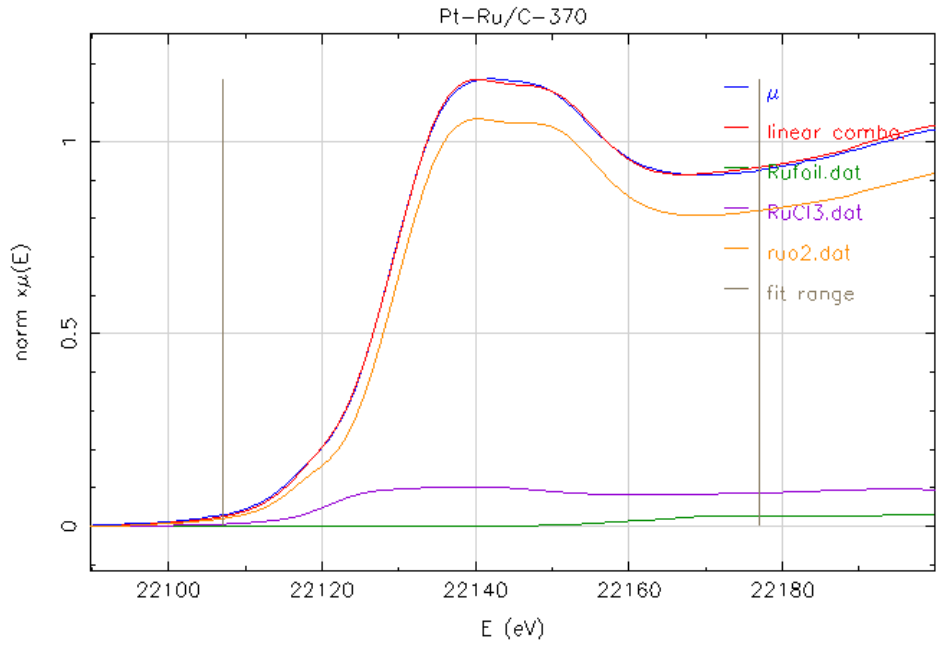
Pt-Ru/C-370
norm xμ(E)
E (eV)
μ
linear combo
Rufoil.dat
RuCl3.dat
ruo2.dat
fit range

(i)

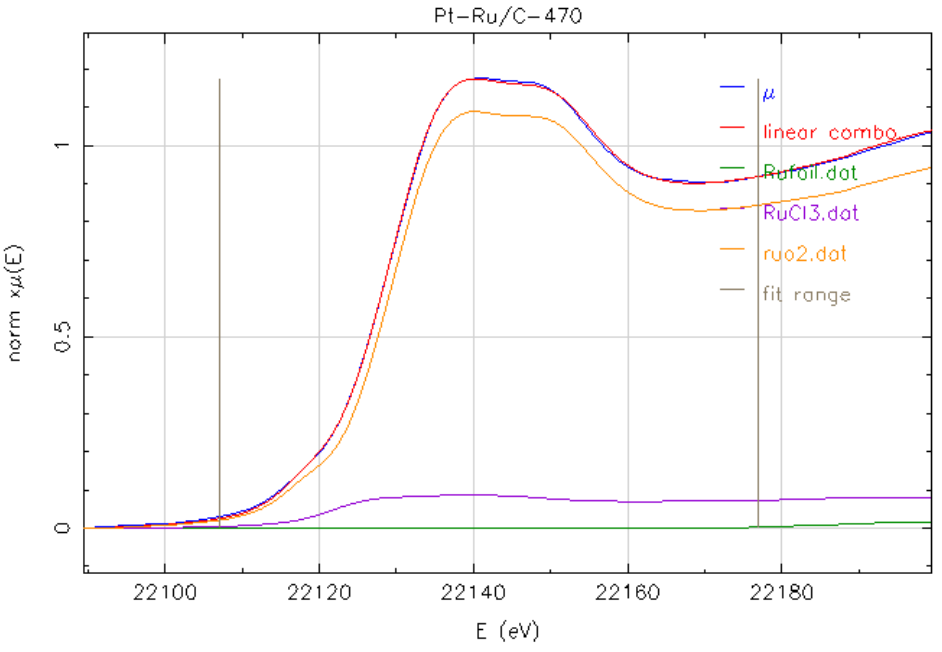
Pt-Ru/C-470
norm xμ(E)
E (eV)
μ
linear combo
Rufoil.dat
RuCl3.dat
ruo2.dat
fit range

(j)

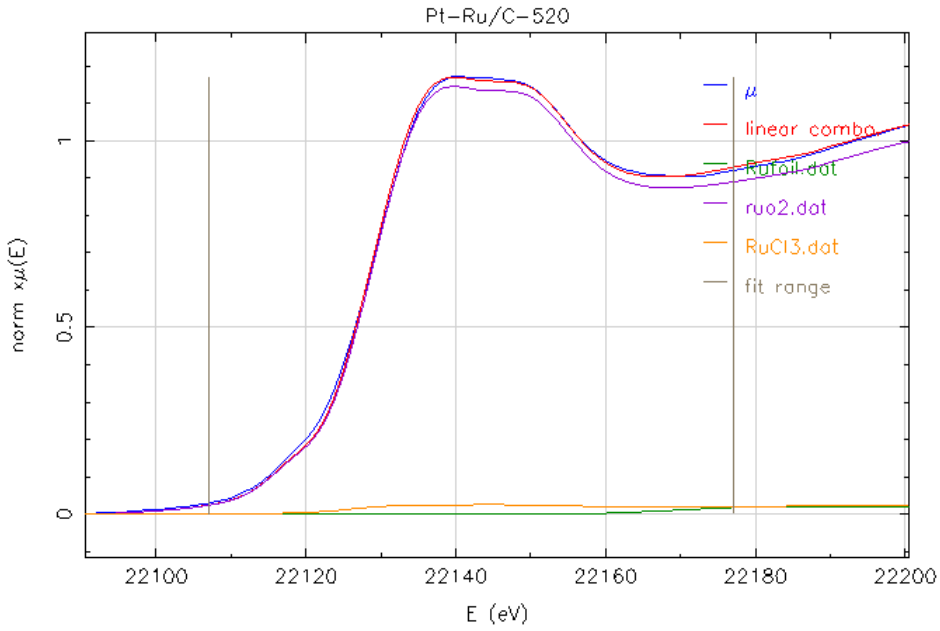

(k)

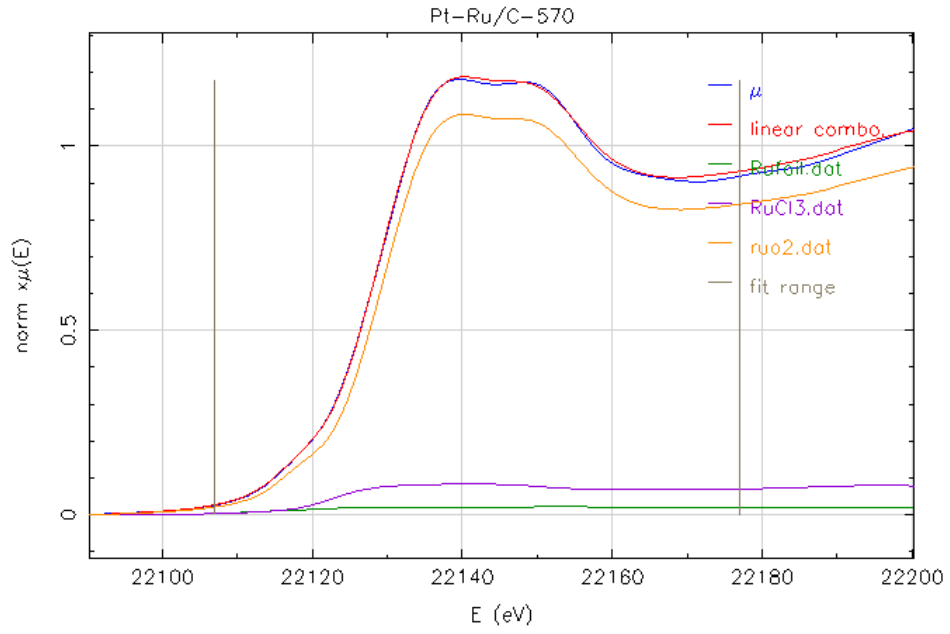

(l)

Figure S2. Least-square linear combination fitting curves of $Pt-Ru/C$ samples at Pt L_3 (a – f) and Ru K-edges (g – l) under different T_o treatment. The obtained fitting curves are in good agreement with the experiment XANES profile.

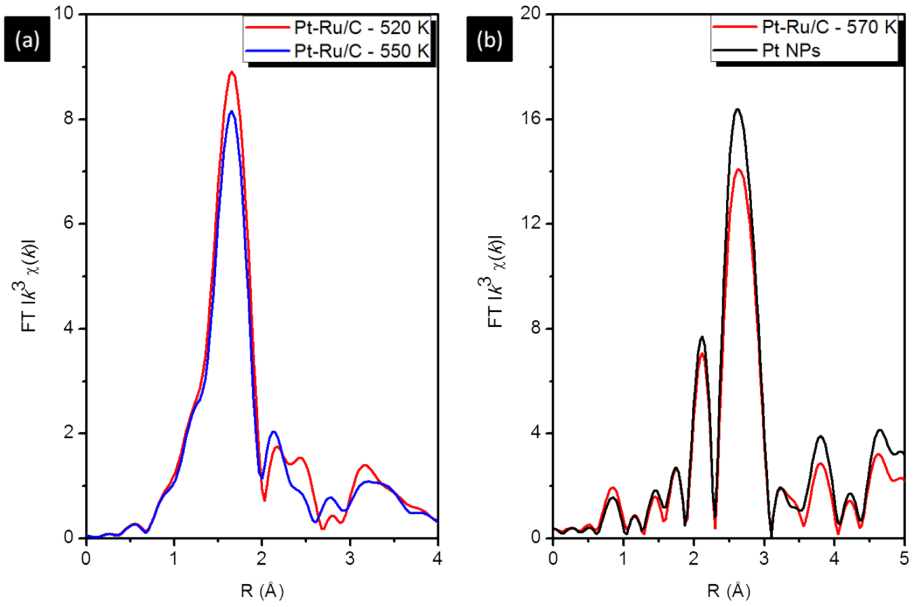

Figure S3. Overlain of R – space EXAFS spectra for 520 K and 550 K samples.

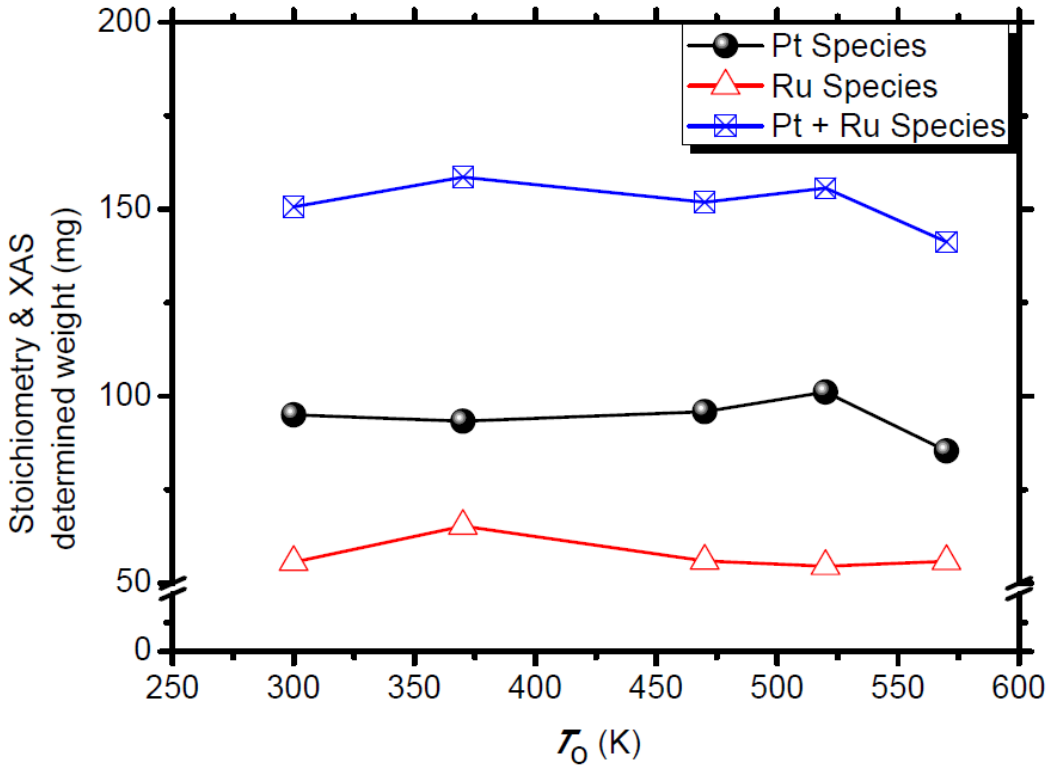

Figure S4. The estimated total weights of Pt and Ru species of $Pt-Ru/C$ samples under different oxidation temperature (T_o). Pt species include metallic Pt, PtO_2, and

$PtCl_4$, all of which are the products of the eq. S6 and S7. Similarly, Ru species include Ru, RuO_2 and $RuCl_4$.

S3.1. Density functional theory simulation

The surface binding/absorption energy of oxygen molecules are calculated to predict the oxygen dissociation associating with the methanol oxidation activity of oxidized $Pt-Ru/C$ using the DFT calculation with the pseudopotentials and the plane-waves basis sets. During the calculation, the exchange–correlation effects are treated by the Perdew–Burke–Ernzerhof functions. The electron cores are described by Vanderbilt's ultrasoft pseudopotentials for Pt, Ru, and O atoms. Our calculations were conducted out using the Quantum ESPRESSO computer code.[26] In order to simplify the calculation, there are two kinds of substrates on which the oxygen molecules are horizontally absorbed. The first substrate, Pt/(001)RuO_2, comprising one layer of Pt atoms at the top and three atomic layers of (001) rutile RuO_2 crystal as a sublayer. The second one, Pt/(0001)Ru, consisted of one Pt atoms top layer and a three-atomic-layers (0001) Ru hexagonal close packed (h.c.p.) substrate. For the first substrate, the lattice constants of RuO_2 are a = 4.492 Å and b = 3.107 Å. Its corresponding supercell is orthorhombic of size 8.98 Å x 8.98 Å x 25 Å. The lattice constants of Ru h.c.p. crystal are a = 2.755 Å and c = 4.28 Å corresponding to an orthorhombic supercell of 8.267 Å × 9.545 Å × 25 Å. Periodic boundary condition is applied for both supercells with the separating vacuum regions of about 15 Å. The Brillouin zones of

the supercells are sampled by a Γ − centered Monkhorst − Pack mesh of 8 × 8 × 2 **k** − points together with a first − order Methfessel − Paxton smearing of width 0.2 eV. The wave functions are expanded in plane waves (PWs) basis set with the kinetic energy cutoff of 400 eV (~ 29 Ry). Finally, the structural optimization of each chemisorption geometry was performed using the Broyden − Fletcher − Godfarb − Shanno algorithm. During optimization, atoms at the three bottom layers are kept fixed at their truncated bulk positions while the Pt atoms and the oxygen molecules are set to relax. The relaxation terminates when the total energy is converged within the threshold of 10^{-8} eV.

S4. Electrochemistry experiments.

Linear sweep voltammetry experiments were performed on the $Pt-Ru/C-T_o$ samples to monitor their MOR activity. The working electrodes were ca. 3 mg of sample prepared by blade casting method with the slurry of $Pt-Ru/C$ powder mixing with adequate amounts of isopropanol and Nafion − 117 electrolytes. Electrical contact was made to the electrode with a platinum wire sealed in a glass tube. A three − electrode setup was used in a three-compartment all glass electrochemical cell. The reference electrode used was a normal hydrogen electrode (NHE), and the counter electrode used was a piece of 10 × 10 mm^2 standard foil of platinum. The electrolyte was a mixture of 1.0 M H_2SO_4 and methanol because of its high conductivity and H^+

molecule ions to participate in the MOR reactions. All potentials were referenced to the NHE. The spectra were collected at a potential sweeping rate of 10 mV s^{-1} and all experiments were conducted at 22 ± 3°C. The instrument used for these measurements was a CH Instruments Model 600B potentiostat under chi627d software control. The details of electrochemical experiments were reported in the previous studies.[1]

S4. TGA analysis:

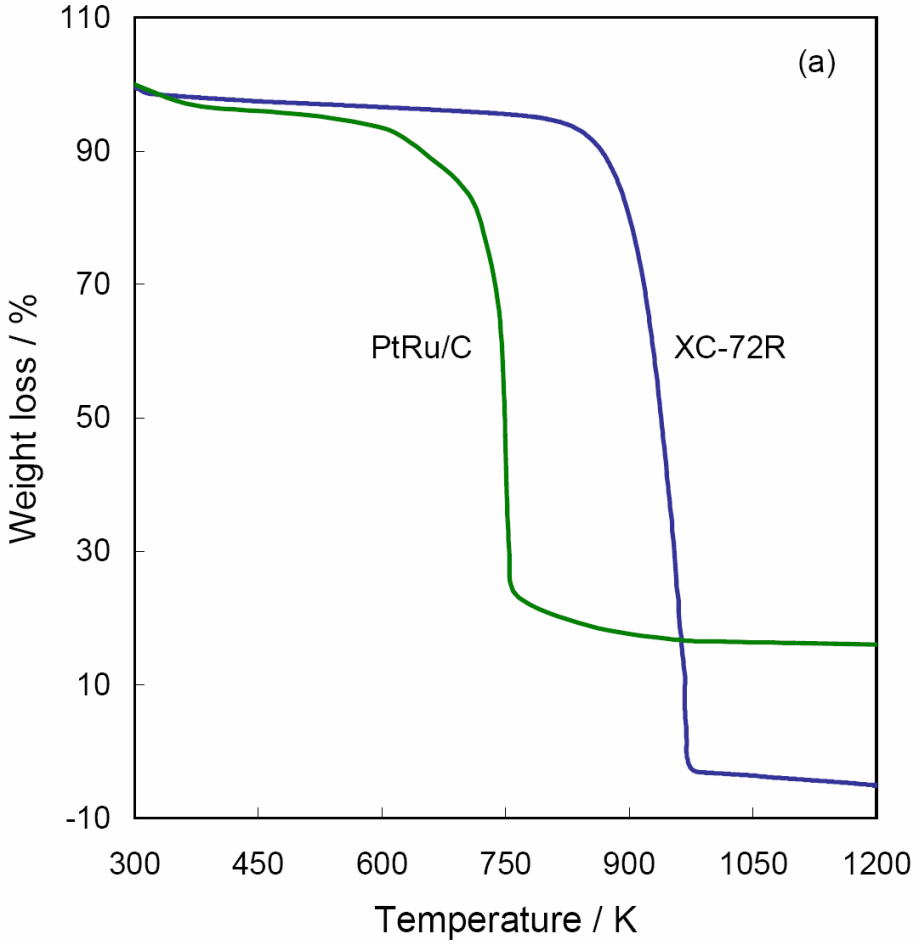

Figure S5. Thermal Gravity analysis curves of $Pt - Ru/C$ sample and blank carbon support

Reference:

1. Huang, S. Y.; Chang, S. M.; Yeh, C. T., Characterization of surface composition of platinum and ruthenium nanoalloys dispersed on active carbon. *The Journal of Physical Chemistry B* **2006,** *110* (1), 234-239.
2. Langford, J. I.; Wilson, A. J. C., Scherrer after sixty years: A survey and some new results in the determination of crystallite size. *Journal of Applied Crystallography* **1978,** *11*, 102-113.
3. Newville, M., IFEFFIT: interactive XAFS analysis and FEFF fitting. *Journal of Synchrotron Radiation* **2001,** *8*, 322-324.
4. Ravel, B.; Newville, M., ATHENA, ARTEMIS, HEPHAESTUS: data analysis for X-ray absorption spectroscopy using IFEFFIT. *Journal of Synchrotron Radiation* **2005,** *12*, 537-541.
5. Haines, J.; Leger, J. M.; Schmidt, M. W.; Petitet, J. P.; Pereira, A. S.; da Jornada, J. A. H.; Hull, S., Structural characterisation of the Pa3- -type, high pressure phase of ruthenium dioxide. *Journal of Physics and Chemistry of Solids* **1998,** *59*, 239-243.
6. Newville, M.; Livins, P.; Yacoby, Y.; Rehr, J. J.; Stern, E. A., Near-Edge X-Ray-Absorption Fine-Structure of Pb - a Comparison of Theory and Experiment. *Physical Review B* **1993,** *47* (21), 14126-14131.
7. Hwang, B. J.; Sarma, L. S.; Chen, J. M.; Chen, C. H.; Shih, S. C.; Wang, G. R.; Liu, D. G.; Lee, J. F.; Tang, M. T., Structural models and atomic distribution of bimetallic nanoparticles as investigated by X-ray absorption spectroscopy. *Journal of the American Chemical Society* **2005,** *127* (31), 11140-11145.
8. Liu, Y.-T.; Wang, M. K.; Chen, T.-Y.; Chiang, P. N.; Huang, P. M.; Lee, J.-F., Arsenate sorption on lithium/aluminum layered double hydroxide intercalated by chloride and on gibbsite: Sorption isotherms, envelopes, and spectroscopic studies. *Environmental Science & Technology* **2006,** *40* (24), 7784-7789.
9. Durham, P. J., X-ray Absorption: Principles, Applications, Techniques of EXAFS, SEXAFS and XANES;. In *X-ray Absorption: Principles, Applications, Techniques of EXAFS, SEXAFS and XANES;*, Koningsberger, D. C.; Prins, R., Eds. John Wiley & Sons: New York, 1998; Vol. 92, pp 53-81.
10. Ankudinov, A. L.; Ravel, B.; Rehr, J. J.; Conradson, S. D., Real-space multiple-scattering calculation and interpretation of x-ray-absorption near-edge structure. *Physical Review B* **1998,** *58* (12), 7565-7576.
11. Rehr, J. J.; Albers, R. C., *Phys. Rev. B.* **1990,** *41*, 8139-8149.
12. Moore, W. J.; Pauling, Ÿ. L., *Journal of the American Chemical Society* **1941,** *63*, 1392-1394.
13. Boman, C. E., Refinement of Crystal Structure of Ruthenium Dioxide. *Acta*

Chemica Scandinavica **1970,** *24* (1), 116.
14. Ravel, B., ATOMS: crystallography for the X-ray absorption spectroscopist. *Journal of Synchrotron Radiation* **2001,** *8*, 314-316.
15. Chen, T.-Y.; Lin, T.-L.; Luo, T.-J. M.; Choi, Y.; Lee, J.-F., *Chemphyschem* **2010,** *11*, 2383-2392.
16. McKeown, D. A.; Hagans, P. L.; Carette, L. P. L.; Russell, A. E.; Swider, K. E.; Rolison, D. R., Structure of Hydrous Ruthenium Oxides: Implications for Charge Storage. *The Journal of Physical Chemistry B* **1999,** *103*, 4825-4832.
17. Chakroune, N.; Viau, G.; Ammar, S.; Poul, L.; Veautier, D.; Chehimi, M. M.; Mangeney, C.; Villain, F.; Fievet, F., Acetate- and Thiol-Capped Monodisperse Ruthenium Nanoparticles: XPS, XAS, and HRTEM Studies. *Langmuir* **2005,** *21*, 6788-6796.
18. Zhan, B.; White, M. A.; Sham, T.; Pincock, J. A.; Doucet, R. J.; Rao, K. V. R.; Robertson, K. N.; Cameron, T. S., Zeolite-Confined Nano-RuO_2: A Green, Selective, and Efficient Catalyst for Aerobic Alcohol Oxidation. *Journal of the American Chemical Society* **2003,** *125*, 2195-2199.
19. Falqui, M. T., *Annali di Chimica (Roma)* **1958,** *48*, 1160-1167.
20. Hoekstra, H. R.; Siegel, S.; Gallagher, F. X., *Advances in Chemistry Series* **1971,** *98*, 39-53.
21. Pinheiro, A. L. N.; Zei, M. S.; Ertl, G., Electro-oxidation of carbon monoxide and methanol on bare and Pt-modified Ru(1010) electrodes. *Physical Chemistry Chemical Physics* **2005** *7*,1300-1309.
22. Hoster, H. E.; Janik, M. J.; Neurock, M.; Behm, R. J., Pt promotion and spill-over processes during deposition and desorption of upd-H_{ad} and OH_{ad} on Pt_xRu_1x/Ru(0001) surface alloys. *Physical Chemistry Chemical Physics* **2010,** *12*, 10388-10397.
23. Bligaard, T.; Nørskov, J. K., Ligand effects in heterogeneous catalysis and electrochemistry. *Electrochimica Acta* **2007,** *52* 5512-5516.
24. van Hove, M. A.; Koestner, R. J.; Stair, P. C.; Biberian, J. P.; Kesmodel, L. L.; Bartos, I.; Somorjai, G. A., *Surface Science* **1981,** *103* 189.
25. Durham, P. J., XANES theroy. In *X-ray Absorption: Principles, Applications, Techniques of EXAFS, SEXAFS, and XANES*, Koningsberger, D. C.; Prins, R., Eds. John Wiley & Sons: New York, 1998; pp 53-81.
26. Giannozzi, P.; Baroni, S.; Bonini, N.; Calandra, M.; Car, R.; Cavazzoni, C.; Ceresoli, D.; Chiarotti, G. L.; Cococcioni, M.; Dabo, I.; Dal Corso, A.; Fabris, S.; Fratesi, G.; de Gironcoli, S.; Gebauer, R.; Gerstmann, U.; Gougoussis, C.; Kokalj, A.; Lazzeri, M.; Martin-Samos, L.; Marzari, N.; Mauri, F.; Mazzarello, R.; Paolini, S.; Pasquarello, A.; Paulatto, L.; Sbraccia, C.; Scandolo, S.; Sclauzero, G.; Seitsonen, A.

P.; Smogunov, A.; Umari, P.; Wentzcovitch, R. M., QUANTUM ESPRESSO: a modular and open-source software project for quantum simulations of materials. *Journal of Physics: Condensed Matter* **2009,** *21*, 395502

27. Huang, S. Y.; Chang, S. M.; Lin, C. L.; Chen, C. H.; Yeh, C. T., Promotion of the electrochemical activity of a bimetallic platinum-ruthenium catalyst by oxidation-induced segregation. *The Journal of Physical Chemistry B* **2006,** *110* (46), 23300-23305.